Journal of Magnetic Resonance 211 (2011) 121–133

Contents lists available at ScienceDirect

Journal of Magnetic Resonance

journal homepage: www.elsevier.com/locate/jmr

Realignment capability of the nCPMG sequence

P. Le Roux [a,*], G. McKinnon [b], Y.-F. Yen [c], B. Fernandez [d,e,f,1]

[a] Global Applied Science Laboratory, GE Healthcare, Palaiseau, France
[b] Global Applied Science Laboratory, GE Healthcare, Milwaukee, WI, USA
[c] Global Applied Science Laboratory, GE Healthcare, Menlo-Park, CA, USA
[d] Global Applied Science Laboratory, GE Healthcare, Nancy, France
[e] IADI Laboratory, Nancy-Universite, France
[f] U947, INSERM, Nancy, France

ARTICLE INFO

Article history:
Received 3 February 2011
Revised 4 May 2011
Available online 15 May 2011

Keywords:
Carr–Purcell–Meiboom–Gill (CPMG)
nCPMG
Driven equilibrium Fourier transform (DEFT)
MLEV
Shinnar–LeRoux

ABSTRACT

The nCPMG sequence is based on a particular phase modulation of the refocusing pulse train, and was originally designed for rendering the spin echo amplitude insensitive to the initial magnetization phase. This pulse sequence has the peculiarity of being easily invertible, which enables perfect driven equilibrium experiments, in the absence of relaxation. This magnetization 'realignment' is effective for all three components. Hence the overall operation is transparent. Supporting theory is presented here, together with the first direct experimental proof of the claim. The experiment shows that, with the present stabilization sequence, perfect realignment is indeed made possible for a range of refocusing pulse nutation angles from 130° to 230°.

1. Introduction

The inability of a long train of spin echoes to maintain the bulk magnetization for any initial condition, even when the Carr–Purcell–Meiboom–Gill (CPMG) [1] criteria are fulfilled, is often overlooked. Indeed the CPMG sequence maintains only the magnetization which stays aligned with the axis of the RF refocusing pulse. The other components are rapidly dispersed. To counter this, some pulse train phase modulation schemes have been proposed (XY, MLEV, etc.) [2,3], but they are useful only over a very restricted range, close to π, of the refocusing pulse nutation angle. We have explored more general kinds of phase modulation but concentrated on quadratic phase modulation [4] after rediscovering the work of Murdoch [5], and also, in another context, that of Zur et al. [6]. A stabilization or preparation period was prepended to obtain a constant signal [7]. Then the refocusing property of the quadratic modulation along with diverse practical properties, such as the eigenstates, stabilization, and reconstruction, were presented in Ref. [8]. The technique was applied several times in the context of diffusion imaging [9–11]. More recently the eigenstate symmetry property which allows a perfect refocusing of all magnetization components was explored [12]. The first experimental verifications of this proposal [13] was in the context of hyperpolarized ^{13}C imaging, and was applied to preserve the longitudinal magnetization from excitation to excitation. This experiment used a phase modulation which was only applicable to nutation angles above 160°, due to the design using an analytical first order development [14]. The proof was thus indirect, relying on longitudinal magnetization, and also not totally convincing because the difference in behavior between a train of 160° and a train of 180° refocusing pulses is not very large. A more effective realignment method has been recently described, starting from a more effective stabilization which enables transverse magnetization realignment with nutation angles as low as 130° [15]. This was demonstrated only with simulation results. Here, an experimental demonstration is presented, along with implementation details and a more detailed exposition of the theoretical justification.

2. Theory

It is possible to explain the principle of realignment without resorting to too much mathematics and also without using the spinor or the quantum mechanics framework. Thus in order to reach a wider audience the magnetization vector context is used. For certain situations, though, the spinor approach, as used in the original nCPMG articles, is to be preferred – but such details are relegated to an appendix in order to simplify the main discourse.

* Corresponding author. Address: 129 av. du gen. Leclerc 91120 Palaiseau, France.
E-mail address: patrick.leroux@med.ge.com (P. Le Roux).
[1] Present address: GE Healthcare, Oskar-Schlemmer-Strasse 11, 80807 Munich, Germany.

1090-7807/$ - see front matter © 2011 Elsevier Inc. All rights reserved.
doi:10.1016/j.jmr.2011.05.005

2.1. The nCPMG sequence, an overview

2.1.1. The CPMG basis

Fig. 1 shows a simplified nCPMG sequence without an explicit stabilization period. Apart from the variable phase setting of each individual RF refocusing pulse, represented by a dotted parabola on the top graph, nothing distinguishes it from a normal CPMG sequence. The figure is simplified because we discarded all the selection gradients. Indeed, one can always suppose that we are considering only a sub-slice for a selective *RF* pulse, and assume the pulses to be non-selective (hard pulses). The imaging phase encoding gradients are also discarded. These gradient lobes must be self compensated in any interval which separates one *RF* refocusing pulse from the next, the echo-space, and do not influence the dynamics of the magnetization. Thus only the read gradient is kept in the graph. It may represent the actual read gradient used in the sequence, but more generally it represents all the influences experienced by the magnetization during an echo-space, including the crusher gradients, the chemical shift or B_0 inhomogeneity, and so on. The time integral of all these influences is assumed to be constant for all echo-spaces. Furthermore half of this time integral must be reproduced in the period separating the flip pulse from the first refocusing pulse. In effect, as the chemical shift is not controllable and is continuously acting, this necessitates that the time separating the flip pulse from the first refocusing pulse must be half the echo-space. This can be considered as the first CPMG condition. We denote this time lapse by T, and the time integral of all influences in this period, at a given position, by ωT. This latter term stresses the fact that although gradient and particularly dynamic gradients are involved in imaging, there is no difference between that and a pure spectroscopy experiment, as far as the magnetization at echo and *RF* refocusing pulse times is concerned. We will call the angle ωT the *free precession offset*. Also, only the range of values $0 < \omega T < 2\pi$ need to be treated if the *RF* pulses are considered as hard, instantaneous, pulses. There is then no way to distinguish two magnetization elements whose free precession offsets are separated by 2π. We define also the 'crushing' wavelength as the distance separating two positions such that the free precession offset difference is 2π. In Fig. 1 we also depicted the read gradient during one echo space as composed of two distinct trapezoids with equal shape and area ωT, whereas in reality it will probably be composed of one unique trapezoid. This is to stress the importance of the echo to echo behavior rather than the pulse to pulse behavior. We enumerate the echoes at the different positions by E_i with, by convention, E_0 being that at the center of the flip pulse, which obviously in case of a standard CPMG sequence is not measurable.

The second CPMG condition states that the *RF* refocusing pulse phases be constant, and that the excitation pulse phase be at a at 90° phase difference. While this is generally easy to satisfy with modern hardware, there are cases where this CPMG condition cannot be guaranteed, such as in diffusion imaging. Here, in the event of even minuscule amounts of patient motion, the large phase modulation caused by the diffusion sensitization gradients, typically several hundreds of cycles per millimeter, can never practically be returned to near zero. Hence the magnetization phase at the time of echo 0 may be several 2π turns over an image, even with perfect hardware. This causes signal null artefacts in the reconstructed image wherever the initial magnetization angle is 90°. In this case, the nCPMG sequence may be of interest.

2.1.2. The nCPMG sequence, aim and principle

The nCPMG sequence tries to obtain a useful signal, i.e. a bulk transverse magnetization at each echo, independent of the magnetization phase angle at echo E_0. Contrarily to other solutions available [16,17] it retains a full signal to noise ratio. It is assumed that the initial magnetization phase angle can vary in space, but it must do so slowly enough such that the original magnetization can still be considered as constant inside the 'crushing' wavelength. For instance, in imaging sequences the crushing wavelength is at least the resolution along the read direction, say about one millimeter. In a diffusion experiment, the magnetization phase at the beginning of the nCPMG imaging sequence can vary by about one turn every two or three centimeters. So in this case, the hypothesis of slow variation in space is valid. Conversely, in the case of a sequence not presenting any geometrical selection, as in the case of a pure spectroscopy experiment where the voxel is the object volume itself, one may have to add crushers around each refocusing pulse for the nCPMG sequence to behave as expected.

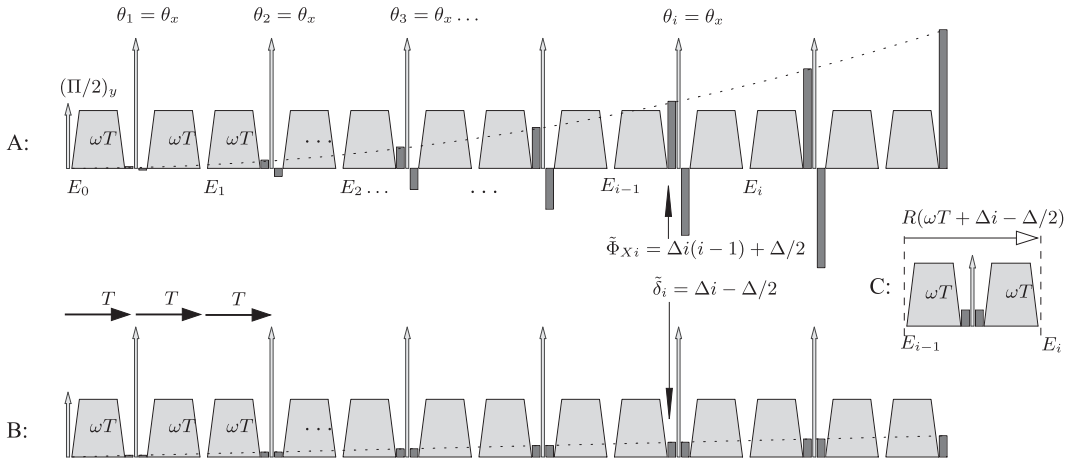

Fig. 1. The top row (A) depicts a typical FSE sequence with a quadratic phase modulation (with second order coefficient Δ) of the phase of the refocusing pulses. In a general manner, varying the emission phase $\tilde{\Phi}_x(i)$ of the pulse can always be modeled by a nutation along a fixed axis x with a precession before and after the pulse, but with reversed sign. These instantaneous, controllable, rotations are depicted by dark boxcar pulses. This is distinguished from the free natural precession due to chemical shift (ω), or main field gradients, represented by light gray trapezoids of time integral value ωT in a half echo space duration T. As far as the action of RF pulses are concerned only the sum of all precession between each pulse is of physical significance. Hence the boxcars precessions can be replaced by symmetric precession around each pulse (this involves changing the receiver phase during the reception, for more details see Fig. 2). For a quadratic phase modulation, one finds that these controlled precessions are varying linearly with the echo index i (bottom row, B). Combining these precessions with the free precession at each side of a given refocusing pulse i makes the rotation from echo E_{i-1} to echo E_i (middle row C) a function of $\omega T + \Delta i$ only (not a function of ωT and Δi separately). This is the basis of nCPMG as one can find states which 'shift' along the free precession direction at a speed $d\omega T = -\Delta$ per echo, like the rotation itself (see Fig. 3).

Fundamentally, nCPMG uses a phase modulation of the refocusing *RF* pulses train; indeed it is rapidly apparent that a pure amplitude or nutation angle modulation is not sufficient to overcome the destruction of the magnetization. Secondly, nCPMG tries to mimic the behavior that the magnetization would have under a hypothetical train of refocusing pulses whose nutation angle is exactly π. In this case the 'in phase component' of magnetization, that along $\vec{X}$ at echo E_0, would give a constant echo signal, whereas the 'out of phase' component, that along $\vec{Y}$ at echo E_0, would change sign every other echo. We call this ideal behavior 'sustained spin echoes'. Trying to obtain a sustained spin echo for any nutation angle is a reasonable target, as it is already realized at least for the first few echoes, when the refocusing pulse nutation is not too far away from 180°, even without doing any *RF* train phase modulation. Now the first question which has to be answered when using a variable phase ϕ_{xi} of refocusing pulse i, is how to set the receiver phase ϕ_{ri} at each echo? The answer is given by the necessity to obtain the ideal sustained spin echo behavior for a 180° ideal pulse case. Taking an arbitrary magnetization orientation $\vec{X}$ at echo E_0, we set the receiver phase ϕ_{r0} (see Fig. 2) such that $\vec{X}$ gives the maximum signal; then if we want this magnetization to always give this constant maximum signal we have to set the receiver phase according to the orientation the magnetization $\vec{X}$ would occupy at each echo: thus, we just have to follow the orientation of the initial magnetization under the action of perfect 180° phase modulated by ϕ_{xi}. Stated differently (see Fig. 2), we have to insure that each *RF* axis is the bisector of the two adjacent receiver phase settings. In the form of a set of equations we have

$$\begin{aligned} &\phi_{xi} = \phi_{r(i-1)} + \delta_i \\ &\phi_{ri} = \phi_{xi} + \delta_i \\ &\delta_i + \delta_{i-1} = \phi_{xi} - \phi_{x(i-1)}, \end{aligned} \tag{1}$$

where we introduce the precession offset δ_i, which is the angle separating ϕ_{ri} from ϕ_{xi}, and ϕ_{xi} from $\phi_{r(i-1)}$. This value can be called the controlled precession offset, or more succinctly precession offset, because, as it is applied on both sides of an *RF* pulse, it can be integrated with the free precessions ωT which already occur on both sides of a refocusing pulse. The last equation indicates that there is a differentiation step for obtaining the precession offsets δ_i from a given sequence of emission phases ϕ_{xi}. Consequently if the emission phase law is quadratic in the form Δi^2, plus other linear and constant terms that we do not consider for the moment, then the precession offset follows a linear law $\delta_i = \Delta i$, plus an alternating signal which can be eliminated by a good choice of the first receiving phase ϕ_{r0}. This is what is shown in Fig. 1, where the quadratic emission phase modulation of the top (A) diagram is replaced by a totally equivalent linear precession offset modulation as shown at the bottom (B) of Fig. 1. The constant $\Delta/2$ in Fig. 1 will become clear in the next section, but it can be justified by remarking that if one fits the discrete value δ_i at each *RF* refocusing time by a continuous linear function of time, it will pass through zero at the time $t = 0$ of echo 0. Independent of this detail, the middle part of Fig. 1C emphasizes that the echo $(i-1)$ to echo i rotation (we neglect relaxation) $R(\omega T, i)$ is translating regularly by $-\Delta$ along the free precession direction ω T. Indeed we have the expression $R(\omega T,i) = R(\omega T + \Delta i)$, showing that the rotation is not a separate function of ω T and i, but only of $\omega T + \Delta i$.

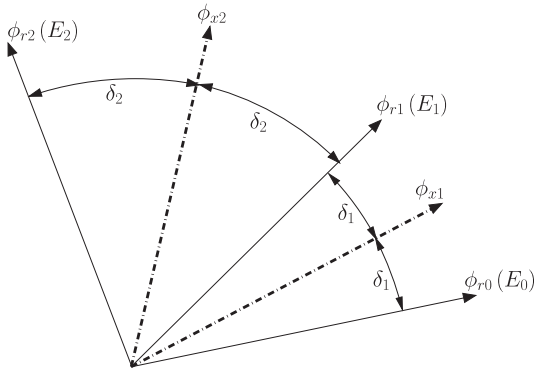

Fig. 2. This figure is a copy of the one published in Ref. [8]. The receiving phase ϕ_{ri} is applied during the reception of echo i, hence following the refocusing pulse i which have emission phase ϕ_{xi}. Of course the echo with index 0 is not measurable, but ϕ_{r0} then represents the reference position of magnetization after the flip pulse. Given the emission phases ϕ_{xi} one can set the receiving phases such that there is the same precession δ_i before and after one pulse i, rendering it equivalent to a varying offset added to the free precession angle ωT. This figure describes graphically Eq. (1). In the case of the first canonical linear precession offset modulation of Fig. 1 the value of precessions are $\delta_1 = \Delta/2$, $\delta_2 = 3\Delta/2 \ldots$.

Notice that the magnetization at a free precession offset $\omega T = -k\Delta$ undergoes the same rotation $R((i-k)\Delta)$ from echo $i-1$ to echo i that the magnetization situated at $\omega T = 0$ has undergone k echo spaces prior. This constitutes a sort of generalization of the linear signal processing result which equates a quadratic phase modulation, or chirp signal, with a linear frequency sweep. We thus call the parameter Δ the (precession) *sweep parameter*. Hence the excitation can be visualized as a 'wave' progressing at a 'speed' $-\Delta$ between each echo. One may like to have the same behavior for the magnetization itself, i.e. one may like to find a repartition of magnetization which translates without modification from echo to echo $\vec{U}(\omega T, i) = \vec{U}(\omega T + i\Delta)$. This distribution will be a good candidate to represent the 'in phase' component as it will give a constant signal along the echo train. Furthermore one can find a distribution $\vec{V}(\omega T, i) = (-1)^i \vec{V}(\omega T + i\Delta)$ which also translates by $-\Delta$ between each echo, but changes sign every other echo. This distribution will be a good candidate for representing the 'out of phase' component. These two distributions $\vec{U}, \vec{V}$, and a third one $\vec{W}$, are called the eigenstates, or eigenfunctions, of the linear sweep. The next Section 2.1.3 succinctly describes how to obtain these distributions. As a guide it may be useful to refer directly to the Fig. 3, left column, which shows these three distributions as if they were at echo E_0. It is in practice impossible to obtain such distributions at echo E_0, just after the flip pulse as only flat distribution $\vec{X}, \vec{Y}$ can then be obtained. It will be the role of a preparation period lasting P echoes to transform these constant distributions $\vec{X}, \vec{Y}$, into the distributions $\vec{U}, \vec{V}$ respectively. This is described in Section 2.1.4.

2.1.3. Determination of the eigenstates

In Ref. [8] we used spinors to determine, among other things, the distributions $\vec{U}(\omega T)$ and $\vec{V}(\omega T)$, but the algorithm can also be transcribed, at least in principle by using direct magnetization and Bloch equation.

The Bloch equation equivalent of the spinor algorithm described in Ref. [8] consists of applying the series of rotations for a particular position, for instance the magnetization at the precession offset $\omega T = 0$. Starting from an arbitrary magnetization vector $\vec{U}_{00}$ one readily obtains by simple matrix multiplication, the sequence $\vec{U}(\omega T = 0, i) = R(i\Delta) \ldots R(\Delta)\vec{U}_{00}$ of magnetization vectors for this particular precession offset, for all the echoes of a cycle $i = 1 \ldots d$. It then suffices, in order to obtain a translating 'wave' in the precession offset domain, to take as initial condition for echo E_0, at the position $\omega T = i\Delta$, the value obtained at position $\omega T = 0$ for echo E_i. Or mathematically $\vec{U}(\omega T = i\Delta, 0) = \vec{U}(\omega T = 0, i)$. Assuming now a sweep factor in the form of a rational $\Delta = 2\pi n/d$, after one completed cycle ($i = d$), one will have to reassign the value $\mathrm{R}(\mathrm{d}\Delta) \ldots \mathrm{R}(\Delta)\vec{U}_{00}$, at position $\omega T = 2\pi$, to the value $\vec{U}_{00}$. This simply forces $\vec{U}_{00}$ to be the axis of the cycle rotation $R(d\Delta) \ldots R(\Delta)$! Thus the three vector components of $\vec{U}_{00}$, and consequently the whole

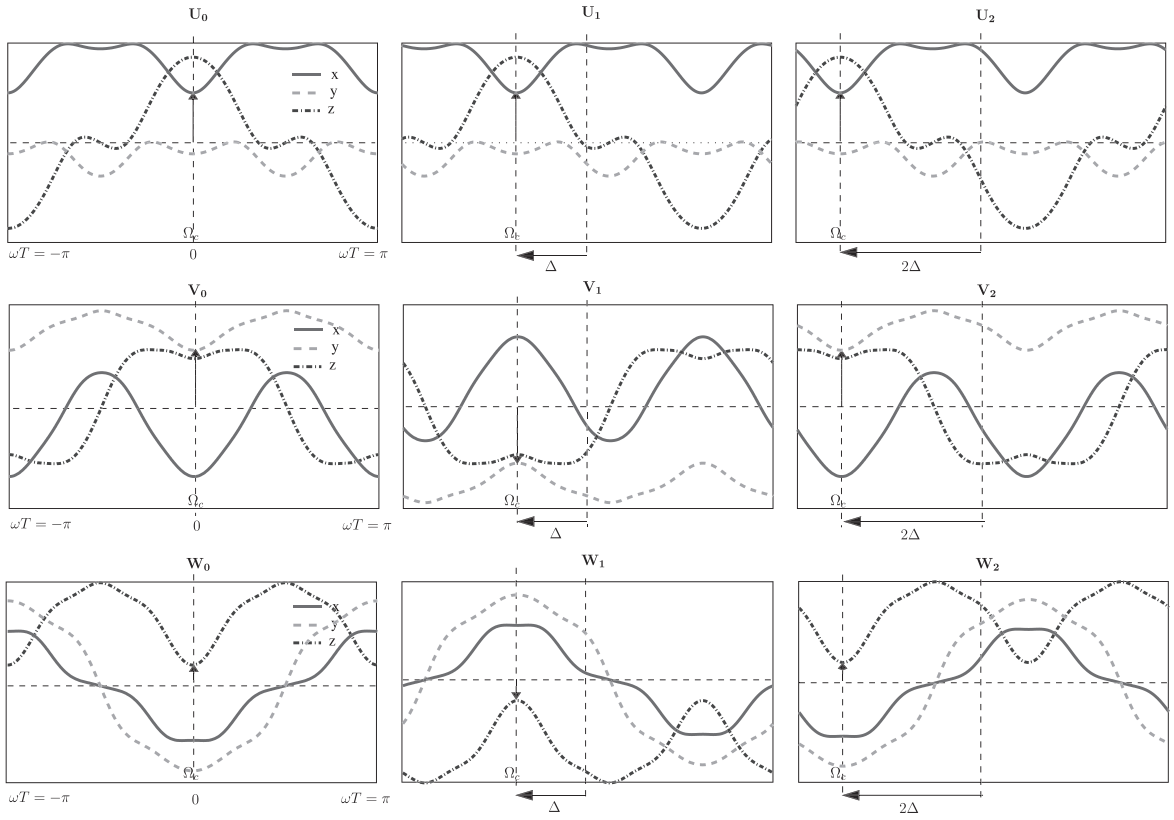

Fig. 3. These graphs are simulation results for the nCPMG sequence with the quadratic modulation with sweep parameter $\Delta = 1.2$ radian. Magnetization response at three successive echoes indexed 0–2, for different free precession value ωT, and for specific initial magnetization distributions $\vec{U}$, $\vec{V}$, and $\vec{W}$, were simulated. The rotation from echo to echo $R(\omega T,i) = R(\omega T + \Delta i)$ corresponds to an action which sweeps regularly at a rate $-\Delta$ by echo space. It is then possible to find magnetization states which themselves are transformed by the rotation in a simple manner. Firstly, the magnetization repartition $\vec{U}(\omega T)$ shown on top row just translates at the same rate $-\Delta$ as the rotation does (echo E_0 at left column to echo number two at right). Secondly the distribution $\vec{V}(\omega T)$ translates at the same rate $-\Delta$, but changes sign every other echo, this is shown on middle row. Another solution translating and changing sign every other echo is $\vec{W}(\omega T)$ shown on bottom row: the difference between $\vec{V}$ and $\vec{W}$ is that $\vec{V}$, as $\vec{U}$, can be generated from a magnetization positioned in the $\vec{X},\vec{Y}$ plane at echo E_0, whereas $\vec{W}$ can be generated starting from a magnetization originally aligned along $\vec{Z}$. One notes a center of symmetry (actually two, separated by π) highlighted by the arrow and the symbol Ω_c.

distribution $\vec{U}(\omega T = i\Delta, 0)$ at echo zero E_0 are determined fully, with only a sign ambiguity. The problem of finding the distribution which gives a constant signal is therefore solved. Finding a vector repartition $\vec{V}(\omega T)$, which translates at a rate $-\Delta$, but simultaneously changes sign at each echo, proceeds in a similar manner, considering again the magnetization at $\omega T = 0$, but with a different initial condition $\vec{V}_{00}$. Its response $\vec{V}(\omega T = 0, i)$ is calculated for all echoes $i = 1,d$, and the result is used to determine initial conditions along the ωT axis as before, but with a minus sign at every other echo. That is $\vec{V}(\omega T = i\Delta, 0) = (-1)^i, \vec{V}(\omega T = 0, i)$. Again, the problem is that at the end of the cycle, or rather at the beginning of the next cycle $i = d$, one must recover the original magnetization $\vec{V}_{00}$. This necessitates $\vec{V}_{00}$ to be another eigenvector of the cycle rotation and that the cycle rotation angle is π if d is odd, or 2π if d is even. This is precisely what was already noticed experimentally by Murdoch [5] and demonstrated in Ref. [8]. However the case $d = 2p$, with its cycle rotation angle equal to 2π, if d is sufficiently large, poses some problems to the algorithm as the rotation axis is ill-defined. One has then to resort to studying the half-cycle. This complicates somewhat the algorithm, but the final result is similar to the case of odd d. That is why in Ref. [8] only odd d was considered; we suppose the same here. The left column of Fig. 3 shows the result of the algorithm for a well-chosen value of Δ close to 1.2 radians or half the (small) golden angle

$$\widehat{\Delta} = \pi\left(1 - \frac{1}{\Phi}\right), \qquad \Phi = \frac{\sqrt{5}+1}{2} \tag{2}$$

For practical purposes it is approximated by $\Delta = 2\pi n/d$ with n and d integers. The denominator d, the period of the modulation, must be large enough ($(\cos\theta/2)^d \ll 1$). In Fig. 3 the nutation angle of the refocusing pulse was $\theta = 2$ rad, and $d = 499$, $n = 95$. Because d is odd there is only one very well defined solution $\vec{U}(\omega T)$, but there are two solutions for $\vec{V}(\omega T)$. We have to combine these two solutions in order to obtain a solution $\vec{V}(\omega T)$ which is a magnetization distribution obtainable by a $(\pi/2)_y$ pulse followed by a train of echoes. To insure this, the x,y components of the vector must be even, $Vxy(\omega T + \pi) = Vxy(\omega T)$, and the z component must be odd $Vz(\omega T + \pi) = -Vz(\omega T)$. One then obtains a distribution $\vec{V}(\omega T)$ but also a complementary distribution $\vec{W}(\omega T)$, which has a parity corresponding to the magnetization originally aligned with $\vec{Z}$ after the flip pulse.

Finally, one can verify on Fig. 3 the action of the quadratic phase modulation on the obtained distributions. For that a very elementary series of rotations, expressed by the Bloch equations, for each precession offset, was used. Hence from echo E_0 to echo E_1, the simulation is composed of a free precession, proportional to ωT, a nutation θ along the ascribed phase ϕ_{x1}, again a precession ωT, and finally observation in the rotating frame defined by ϕ_{r1}. The center column shows the three distributions thus obtained, at echo E_1. The right column shows the result of a second iteration of the previous series of rotations, leading to the distribution at echo E_2. It can be verified that $\vec{U}$ is just translating by $-\Delta, \vec{U}(\omega T, i) = \vec{U}(\omega T + \Delta i)$, whereas $\vec{V}$ and $\vec{W}$ are also translating and in addition, changing sign.

A simple important remark is that if $\vec{U}(\omega T)$, $\vec{V}(\omega T)$, and $\vec{W}(\omega T)$ are the eigenstates for a particular linear sweep, the linear sweep obtained by adding δ_0 to every precession offset δ_i has just the same eigenstates but translated in the precession offset domain by $-\delta_0$, $\vec{U}(\omega T+\delta_0)$, $\vec{V}(\omega T+\delta_0)$, and $\vec{W}(\omega T+\delta_0)$.

2.1.4. The preparation period

Fig. 4 recalls the principle of the stabilization or preparation period. As previously noted the role of the preparation period is to transform constant distributions $\vec{X}$, $\vec{Y}$, into the distributions $\vec{U}$, $\vec{V}$ respectively. The minimum number P of echoes in the preparation period must be adapted to the spatial content of the distributions $\vec{X}$, $\vec{Y}$, which itself depends on the nutation angle. By experience one finds that a preparation period of four echoes is sufficient to align the original flat distributions onto the eigenstates for nutation above 160° only [14]. In the original work [8] a preparation with $P=7$ was used which permitted stabilization, i.e. putting the magnetizations onto the eigenstates, for nutation angles as low as 120°. The linear sweep has then to be delayed by P echoes, beginning at the center of echo P, and the first P refocusing pulses are used to transform each of the three magnetizations $\vec{X}$, $\vec{Y}$, $\vec{Z}$ into the distributions $\vec{U}(\omega T),\vec{V}(\omega T),\vec{W}(\omega T)$ respectively. It is only from the refocusing pulse number $P+1$ that one applies the linear sweep. But it is useful to remark that the sampling of the signal is practical during this preparation period, as it is only the first few echoes that are very unstable.

The preparation of Le Roux [8] was designed by non-linear programming optimization. In Ref. [18] by using a linearization of the spinor equations, a longer stabilization law was designed. Although this new design did not permit a further reduction in the minimum refocusing nutation angle, it did reduce substantially, at say 120°, the residual signal oscillation, due to the more gradual reduction of the mismatch between the magnetization and the eigenstates. It is this last preparation, with indefinite length P, that is used in the experiments presented below. Towards a better understanding of the realignment computation, it is best to first consider a fixed P, such as the value $P=7$ found in Ref. [8]. Then, it will be permissible to use the fact that for such a modulation the value P is only a minimum, and one can always imagine an elongated preparation! Indeed by nature of the evolution, composed of only rotations, the sum of squared difference between the magnetization state and the eigenstates stay constant, once the pure linear sweep is in action. Going further one can always consider a modulation with indefinite P as a constantly improving modulation.

2.1.5. The symmetry property of eigenstates

It is clear from Fig. 3, that there is a symmetry around the position $\omega T=0$ (or $\omega T=\pm\pi$), for each of the three components of the three eigenstates distributions $U\,V\,W$. This symmetry position, noted Ω_c, translates by $-\Delta$ at each subsequent echo. Actually to obtain the symmetry at the position $\omega T=0$, at echo E_0, we had to change the phase modulation law given in Fig. 1, by adding a $\pi/2$ to the precession offset in addition to the 'strange' $\Delta/2$ that we already added

$$\delta_i=\frac{\pi}{2}-\frac{\Delta}{2}+\Delta i,\qquad i=1\ldots \tag{3}$$

Without the added $\frac{\pi}{2}$, the symmetry about $\omega T=0$ (or $\omega T=\pi$) in Fig. 3 would have been about $\omega T=\frac{\pi}{2}$ (or $\omega T=3\frac{\pi}{2}$) and the rest of this paper, which relies on this symmetry, would be more complicated to follow. To mark the special property of the law (3) we call it the *special* or *canonical* linear precession modulation. In order to obtain a sustained spin echo behavior the law (3) supposes that the magnetization is already along one of the eigenstates at echo E_0. In practice a preparation period of length P is needed to insure this, and hence one has to change the index i in (3) to $i-P$, or simply add an offset $\delta_0=-P\Delta$ to the law. Any of these actions translates the start of the linear sweep to echo E_P. We will say that we render the linear sweep *canonical* at echo E_P. The symmetry of the eigenstates was overlooked in Ref. [8] and even the offset $-\Delta/2$ was left uncompensated. That is the reason why the points of symmetry occurred seemingly at a random position in Fig. 5 of Le Roux [8]. But one can always, by addition of a precisely adapted offset δ_0, render any pre-existing modulation canonical at echo E_0 or at the end of its prepration E_P.

The new symmetry can once again be accepted as a fact, but for completeness it is demonstrated in Appendix A, using the spinor formalism of Le Roux [8] with, this time, the special modulation form (3).

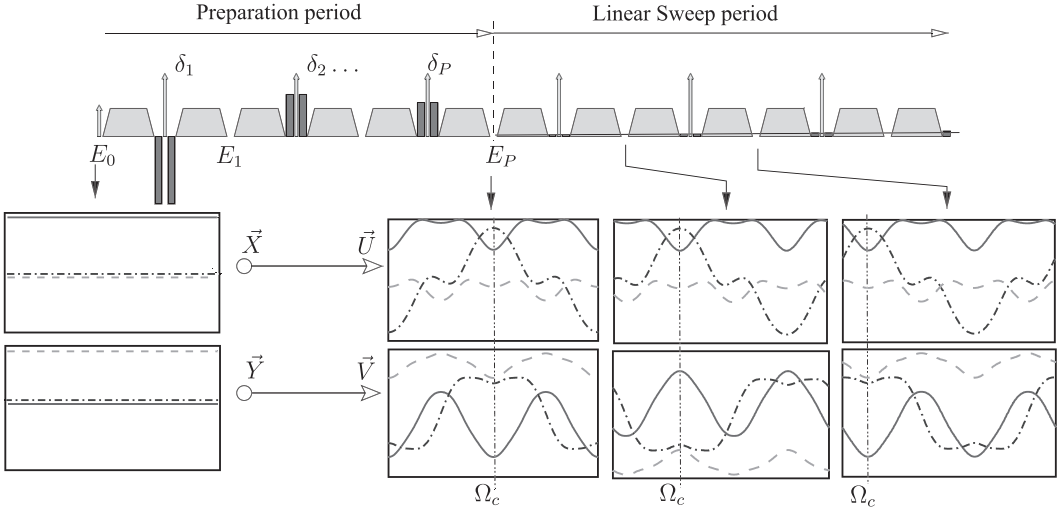

Fig. 4. It is the role of the preparation sequence to transform the original magnetization aligned with $\vec{X}$ after the flip pulse (echo 0) into the distribution $\vec{U}(\omega T)$ and to transform the magnetization originally aligned with $\vec{Y}$ into $\vec{V}(\omega T)$ (a simple argument then shows that $\vec{Z}$ is transformed into $\vec{W}(\omega T)$). From echo P, and *RF* pulse number $P+1$, one can start the original linear sweep modulation and then the distribution $\vec{U}(\omega)$ will evolve by pure translation, giving a constant signal, whereas the $\vec{V}(\omega T)$ distribution, changing sign every other echo, will give a flip-flopping signal.

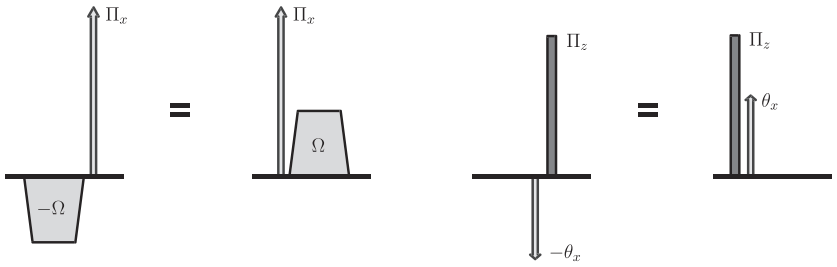

Fig. 5. The commutation rule $\sigma_i\sigma_j + \sigma_j\sigma_i = 2\delta_{ij}$ finds a direct expression in the fact that a π pulse can always be transferred from before to after another rotation, under the condition that the sign of this rotation is changed if its axis is perpendicular to the axis of the π pulse, and obviously doing nothing if the two rotations share the same axis and commute. The figure depicts the two configurations for which this manipulation will be used in the paper, enabling one to reverse the sign of natural precessions, (left) or change the sign of a nutation (right). To enable this manipulation, a 2π (transparent) pulse along a well choosen axis is inserted in the sequence and one half of it (the π pulse) is then translated.

2.2. Inversion, or realignment, of a nCPMG sequence

One is now in position to invert, in the mathematical sense, a nCPMG sequence. That is to say, one is given a nCPMG sequence, including or excluding the $(\pi/2)_y$ pulse, but comprising P preparation pulses, possibly followed by L pulses of linear sweep. One is then asked to find the characteristics of the pulse sequence which would return the magnetization back to its original position, this for all ωT, and for *any original position* of the magnetization, along $\vec{X}$, $\vec{Y}$ or $\vec{Z}$. The term inversion is ambiguous, particularly in the context of MR, hence one will prefer the term realignment. The term realignment was proposed by two of the authors in an earlier development concerning the ability to 'realign' at the end of a nCPMG sequence the $\vec{W}(\omega T)$ distribution to its original position $\vec{Z}$, in the context of prepolarized nuclei [13]. But the term realignment is used more generally here to denote the distribution $\vec{U}(\omega T)$ being transformed back into the constant vector $\vec{X}$, the distribution $\vec{V}(\omega T)$ transformed back into the constant vector $\vec{Y}$, and the distribution $\vec{W}(\omega T)$ being realigned on $\vec{Z}$.

In principle we can include at the end of the refocusing train, a $-(\pi/2)_y$ inverted flip pulse, realizing a generalization of the Driven Equilibrium experiment [19]. And, indeed, it should normally be possible to invert the initial flip pulse, as the constant natural free precession will be compensated at the last echo position. But note that spurious, uncontrolled phase precessions that vary in space, such as those present in a diffusion preparation are not invertible. Thus we here concentrate on the inversion of the refocusing pulse train.

In two occasions during the following section, the usage of the commutation rules, or rather anti-commutation rules, of rotations will be used in order to change the sign of a series of rotations along one axis. The manipulation is illustrated in Fig. 5.

2.2.1. Inversion of a sequence of hard pulses

The top of Fig. 6 shows the naive inversion of the nCPMG preparation sequence, whereby the $\pi/2$ pulse is just a place holder and as such we do not try to invert it. (In fact this section applies to any similar sequence of hard pulses separated by precession.) The naive inversion consists of reversing the order and the sign of all rotations, thus obtaining the identity operator by combination. It is naive because even if the controlled precessions (δ_i) and the nutations, and maybe also the free precessions due to the dynamic gradients, can be inverted, the sign of the constant free precessions due to chemical shift or B_0 inhomogeneity cannot be changed. To alleviate this impossibility, the classical approach consists in adding a 2π pulse, for instance along x, at one end of the sequence. Cutting this $2\pi_x$ pulse into two halves and shifting one of the π_x pulses towards the other end of the sequence, one has to change the sign of all rotations with an axis perpendicular to x in the process, which in the present case means all the precessions according to the commutation rule of Fig. 5. One thus obtains the inversion sequence at the bottom of Fig. 6, shown along with the original preparation sequence. The presence of a perfect π_x pulse at the end of the inversion is not an issue as it can be merged with the inverse of the flip pulse, when present. However the necessity to have a perfect π_x in between the original sequence and its inverse presents a real problem, rendering practical inversion of an arbitrary sequence non realizable.

2.2.2. The simple invertibility of the nCPMG preparation

The nCPMG preparation is special in that it can be very simply inverted as is explained with reference to Fig. 7. With the rotation realized by the preparation sequence being the same for the free precession ωT and its opposite $-\omega T$, one could, at least in principle, realize the same preparation with the same sequence, but with inverted free precession sign (middle row, left, of Fig. 7). Of course this new preparation sequence is not realizable as one cannot invert the sign of the natural part of the free precession. But performing the naive inversion of this (middle row, right, of Fig. 7) reassigns the original sign to all the free precessions, giving a sequence which is realizable. But this latter sequence is also the inverse sequence of the original preparation of the top row of Fig. 7! Hence inverting the original sequence is realizable. For convenience, and to eliminate the need to change the sign of nutation, one can add on the left of each nutation a precession $2\pi_z$, split it in two halves, shift one of the π_z towards the right of the nutation, and change the sign of the nutation according to the commutation rule of Fig. 5. Merging the π_z precessions with the δ_is, one finally obtains the pair of sequences, the preparation and its inverse, shown in Fig. 7, bottom row. This is summarized by the equation linking the two halves of the pair, preparation, realignment which follows:

$$\delta_i = \pi - \delta_{2P+1-i}, \qquad i = P+1, 2P \tag{4}$$

2.2.3. The invertibility of a whole nCPMG sequence

We tackle now the inversion of a whole nCPMG sequence. First, considering the preparation-realignment sequence pair of Fig. 7 and adding $-\Omega_0$ to all the δ_i, $i = 1, 2P$, one notes that, as this is equivalent to a change of central frequency of the system, one would still end up with a preparation and its inverse. Thus the principle of nCPMG inversion does not rely on the symmetry of response between ωT and $-\omega T$, but rather on the existence of such a symmetry somewhere, provided the realignment part and the preparation part are adapted to each other.

Let us suppose now that the preparation of length P is followed by a linear sweep period of L echoes, with L even. At echo $P + L$ the magnetization distributions $\vec{U}$, $\vec{V}$, $\vec{W}$ have been translated by $\Omega_0 = -L\Delta$. One can think of these distributions as being the result

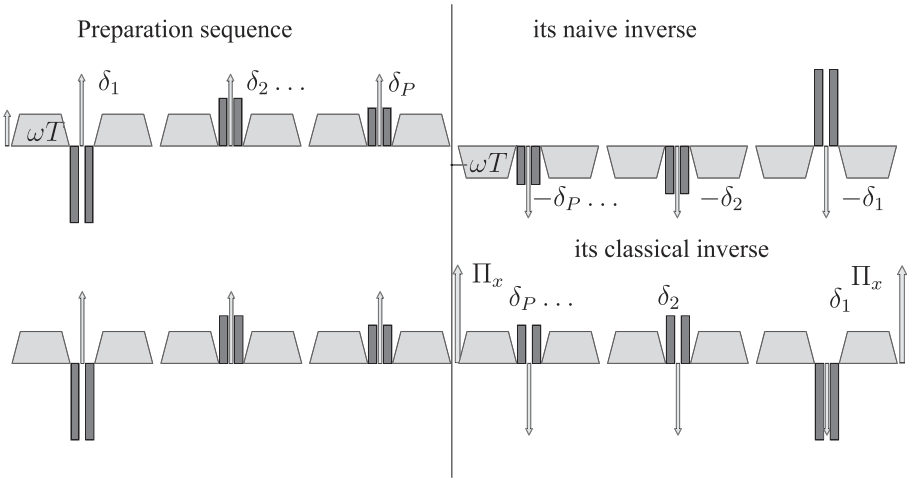

Fig. 6. On the top row is a preparation sequence (but that may in principle be any sequence). The 'naive' inversion of such a sequence would consist in reversing the order of each elementary rotation and changing the sign of the rotation angle of each one. The obvious impossibility to realize this inversion lies in the fact that one cannot change the direction of the free precessions related to main field inhomogeneity or chemical shift! The general available solution, bottom row, consists in adding at the end of the naive inverse a transparent $2(\pi)_x$ hard RF pulse and to slide one half of it toward the beginning, changing in the process the sign of any rotation having its axis perpendicular to $\vec{X}$ (commutation rule). The free precessions regain their natural sign and are thus realizable. But one ends up with the necessity of using two perfect hard π pulses, one at each end of the inversion sequence, so that in practice the inversion is again not realizable.

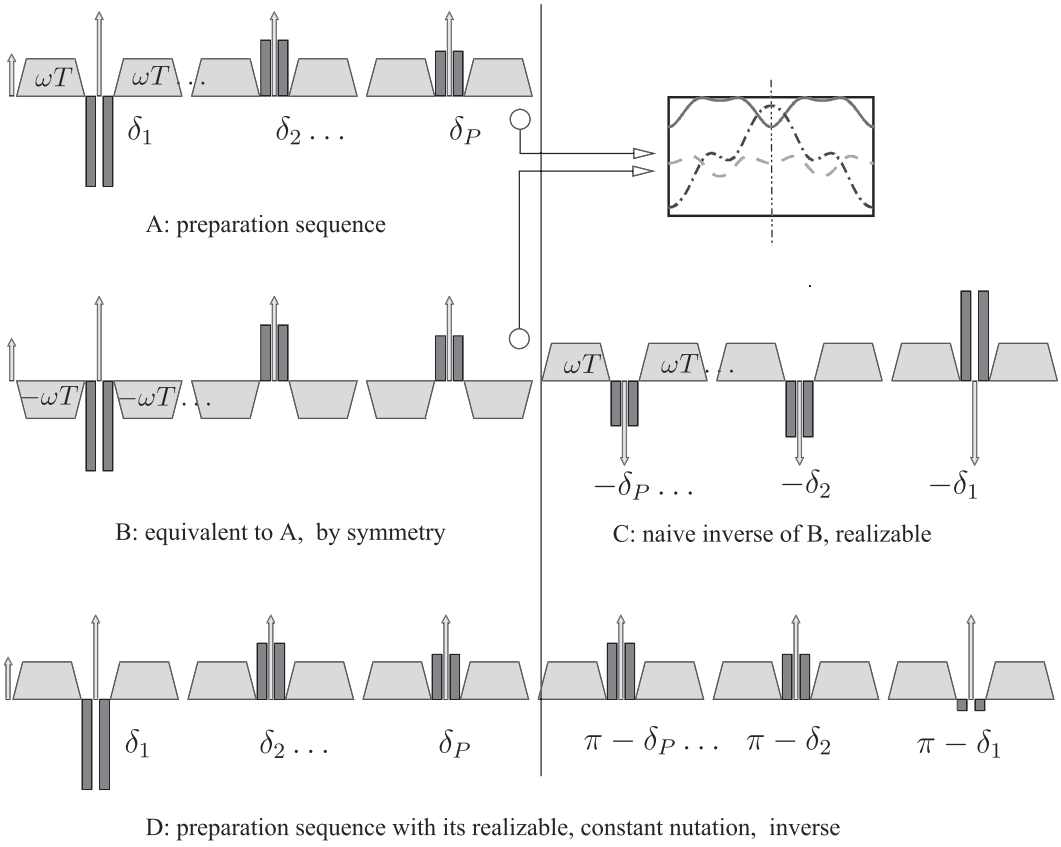

Fig. 7. We consider again the preparation sequence (A) and the problem of its inversion. We make the remark that the rotation applied by (A) is symmetrical around the free precession $\omega T = 0$. Thus the sequence (B) where all the free precessions have been inverted would give exactly the same result. The sequence (B) is not realizable, and consequently its naive inverse is realizable (C). Because (A) and (B) give the same result, the sequence (C) *is also the inverse of (A)*, and the problem is solved. It is just for regaining positive nutations that we add at the end of each nutation a transparent hard precession of $2\pi_z$; then, transferring one half of this precession in front of the nutation (and in consequence changing its sign) we obtain (D), summarizing the preparation sequence with its realizable inverse with constant positive nutations.

of a preparation of P echoes applied from echo L to echo $L + P$, but with the δ_i, $i = 1,P$, augmented by $L\Delta$; so that if one is asked to realign the magnetization starting from echo $L + P$ one just has to apply the P pulses $\delta_i, i = P + 1,2P$ of (4) but augmented by $L\Delta$. This is summarized in Fig. 8.

One will suppose in the remaining of this article that L is even. Indeed a preparation of length P can only put the $\vec{Y}$ component on the direction $(-1)^P\vec{V}(\omega T)$ (and $\vec{Z}$ along $(-1)^P\vec{W}$), and is thus specialized to one parity, and can only be used for deriving an inversion for the very same parity. If L is odd the combination of

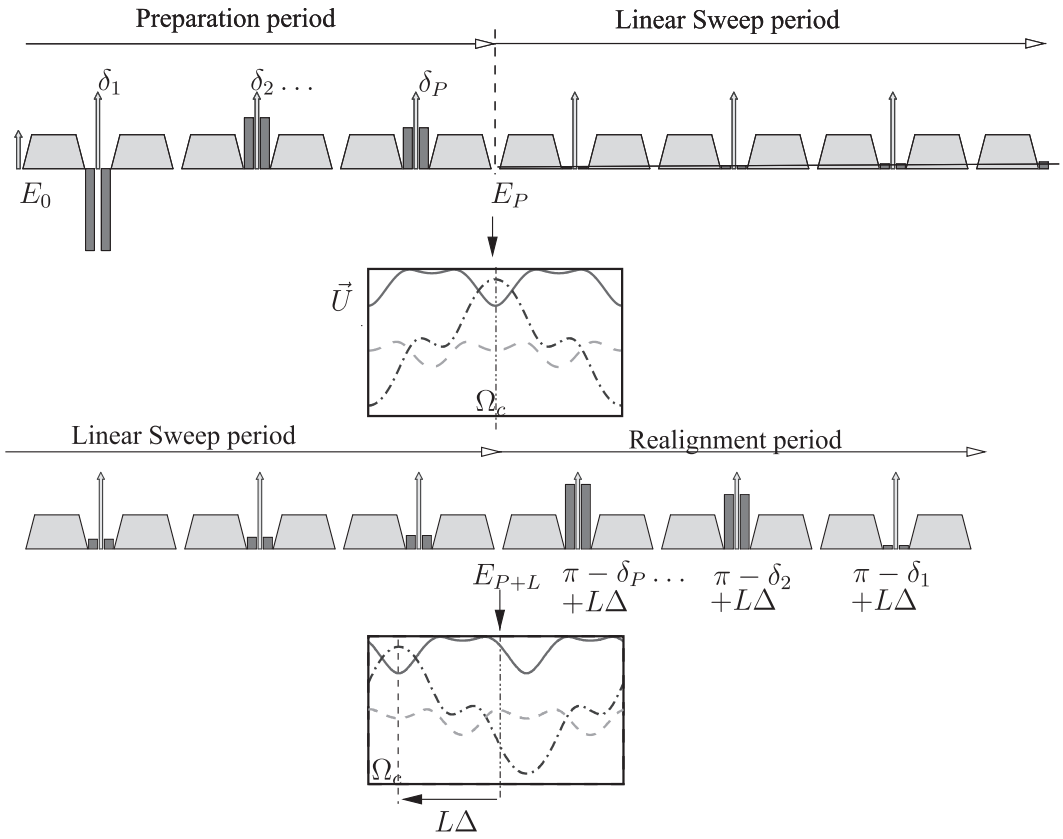

Fig. 8. This figure concerns the case where one wants to realign a linear sweep of length L prepared by a known stabilization period of length P. One can always suppose that L is even, so that the only action of the RF train between echo P and echo $P + L$ is a translation along the free precession axis by $-L\Delta$ (for instance $\vec{U}(\omega T)$ becomes $\vec{U}(\omega T + L\Delta)$). Then it would suffice to add $+L\Delta$ to each free precession of the inversion sequence of Fig. 7 to realign the magnetization.

preparation, linear sweep, and realignment probably leads to an overall operation close to a π rotation around the axis $\vec{X}$. But that cannot be demonstrated with the experimental verification presented below, which relies only on the modulus of magnetization. One notes that for L even the total length of the sequence $N = 2P + L$ is also even. Further, the sequence can be considered as composed of an elongated preparation period of length $P' = P + L/2$, followed directly by its realignment as in Fig. 7. This remark will be useful for handling sequences whereby the preparation period length is not clearly defined, as in Ref. [18].

Table 1
The nutation angle of the refocusing pulse used during the experiment. On the left the nutation that was programmed by manually changing the transmit gain. Only the ratio of the nutation angle was known during the experiment: this is indicated by the values in decibels, following a geometric progression, within 0.1 dB. The value '168°' on the first row was determined by fitting the experimental magnitude responses with theoretical, simulated responses for the row two to four. Due to the high sensitivity of the response corresponding to rows two to four (150° to 118°) we are sure of these nutation values within 2° error range. Nevertheless for reasons unknown we had to adapt slightly the nutation angle from the geometric progression for the highest nutation angle (first row, 168° to 176°), the last one (92° to 89°), and change slightly the next to last. (105° to 106°). The values are summarized on the right column.

Targeted angle	Fitted angle
168°	176°
150° (−1.0 dB)	150°
133° (−2.0 dB)	133°
118° (−3.1 dB)	118°
105° (−4.1 dB)	106°
92° (−5.1 dB)	89°

3. Experimental verification

3.1. Setting

We use the modulation proposed in Ref. [18]. To date, this modulation gives the most stable signals and is used in our imaging experiments. As already noted this modulation sequence has no definite preparation period and hence falls under the remark of the previous section. After having estimated the original offset δ_0, the sequence was rendered canonical at the middle echo $N/2$. The total length N of the sequence was $N = 70$. This elongated 'preparation' period of length $N/2 = 35$ was then realigned in a manner similar to Fig. 7 and according with Eq. (4), with $P = N/2$. The value of $N = 70$ corresponds to a single shot acquisition of a 128×128 image with a half k-space scan. The gradient waveforms of the sequence were similar to those used in imaging [9–11] but with the phase encoding turned off. This sequence was run on a 3T Signa HDxt scanner using version 15.0M4 of the commercial

Table 2
Suite of δ_i, $i = 1, 70$, ($N = 70$), expressed in full 2π turns, after multiplication by 10,000, for the non-realigned sequence used in the experiment. This has been obtained by the difference of the emission and reception phases as given in Ref. [18].

i	δ_i in $2\pi \times 10^{-4}$ radians
1 ... 10	3447, 5141, 7521, 9525, 620, 2730, 5244, 7122, 8835, 862,
11 ... 20	2314, 4420, 6146, 8257, 15, 2016, 4114, 5923, 7911, 9754,
21 ... 30	1787, 3659, 5445, 7507, 9275, 1261, 2967, 5029, 6893, 8770,
31 ... 40	708, 2659, 4613, 6461, 8358, 380, 2164, 4138, 5942, 8020,
41 ... 50	9797, 1738, 3674, 5617, 7518, 9374, 1370, 3278, 5111, 7062,
51 ... 60	8925, 925, 2651, 4692, 6532, 8515, 318, 2311, 4234, 6137,
61 ... 70	8011, 9984, 1893, 3800, 5651, 7656, 9516, 1430, 3294, 5234.

Table 3
Suite of δ_i, $i = 1, 70$, ($N = 70$), expressed in full 2π turns, after multiplication by 10,000, for the realigned sequence used in the experiment. This was obtained from the sequence in Table 2, rendering it canonical at echo $N/2 = 35$ by uniform addition of a suitable value δ_0 and by a realigment computation from echo 35 to echo 70 using the Eq. (4).

i	δ_i in $2\pi \times 10^{-4}$ radians
1 ... 10	6634, 8328, 708, 2711, 3807, 5916, 8430, 309, 2022, 4049,
11 ... 20	5501, 7607, 9332, 1444, 3201, 5203, 7301, 9110, 1098, 2941,
21 ... 30	4974, 6845, 8632, 693, 2461, 4448, 6154, 8216, 80, 1957,
31 ... 40	3894, 5846, 7800, 9648, 1545, 3455, 5351, 7199, 9153, 1105,
41 ... 50	3042, 4919, 6783, 8845, 551, 2538, 4306, 6367, 8154, 25,
51 ... 60	2058, 3901, 5889, 7698, 9796, 1798, 3555, 5667, 7392, 9498,
61 ... 70	950, 2977, 4690, 6569, 9083, 1192, 2288, 4291, 6671, 8365.

software (GE Healthcare, Waukesha, WI, USA). The slice selection was in effect also turned off, by using a slice thickness of 160 mm, whereas the phantom used was a glass test tube of 11 mm diameter, 166 mm long, its long axis aligned with the z axis of the magnet and the acquisition performed at isocenter in a sagittal plane. The test tube was filled just before the acquisition with tap water, with apparent $T_1 = T_2$ in the order of 2.5*s*, and a minimum of 10 s recovery was imposed between each acquisition, dummy calibration included. The read direction was along *z* (long axis of the tube). Each echo signal was composed of 128 points, for a field of view of 24 cm, with a bandwidth of 128 kHz (1000 Hz/pixel). Each signal was Fourier transformed, in effect realizing a projection perpendicular to the long axis of the object. The magnitude of each reconstructed 1.875 mm 'slab' (voxel width) was taken and the magnitude signal of a larger slab representing the central 50 mm of the tube was obtained by taking the square root of the sum of the magnitude squared of each individual slab, yielding a signal $|M_{xy}|_i$ for each of the echoes $i = 1,70$. We repeated this acquisition for the six nutation angles given in Table 1, related in a quasi geometrical progression, with common ratio 8/9 (corresponding to -1.02 dB). The scale factor of the nutation sequence, 168°, was determined a posteriori by model fitting as described at the end of this section. For each nutation angle we performed four acquisitions, two of them with the original [18] modulation whose δ_i are given in Table 2 and two with the realignment modulation of Table 3. For each type of modulation one acquisition was performed with the initial magnetization at echo E_0 along $\vec{X}$: this is the 'in phase' condition. The second acquisition was performed with the initial magnetization along $\vec{Y}$ for 'out of phase' condition.

3.2. Results

The Fig. 9 shows the signals $|M_{xy}|$. The signals are identical for the non-realigned and the realigned sequence during the first half of the echo train. During the second half the modulation with realignment has its precession value deduced from the first half, and it is normal that the signals then differ, but the stability is still guaranteed. The interesting result is of course the very substantial rebuilding of magnetization at the last echo (number 70), corresponding to a magnetization which is almost equal to that obtained with the 180° case. Table 4 summarized the magnitude of signal for all the last echoes, and it can be verified that down to 133° it is equal to the maximum signal, within experimental fluctuations. The magnetization is still reasonably refocused even for the 118° case, which is at the limit of the stabilization capability, with the signal within 3% of the maximum. At least it corresponds to a much higher signal than for the non-realigned case which is between 15% and 20% below the maximum signal attainable.

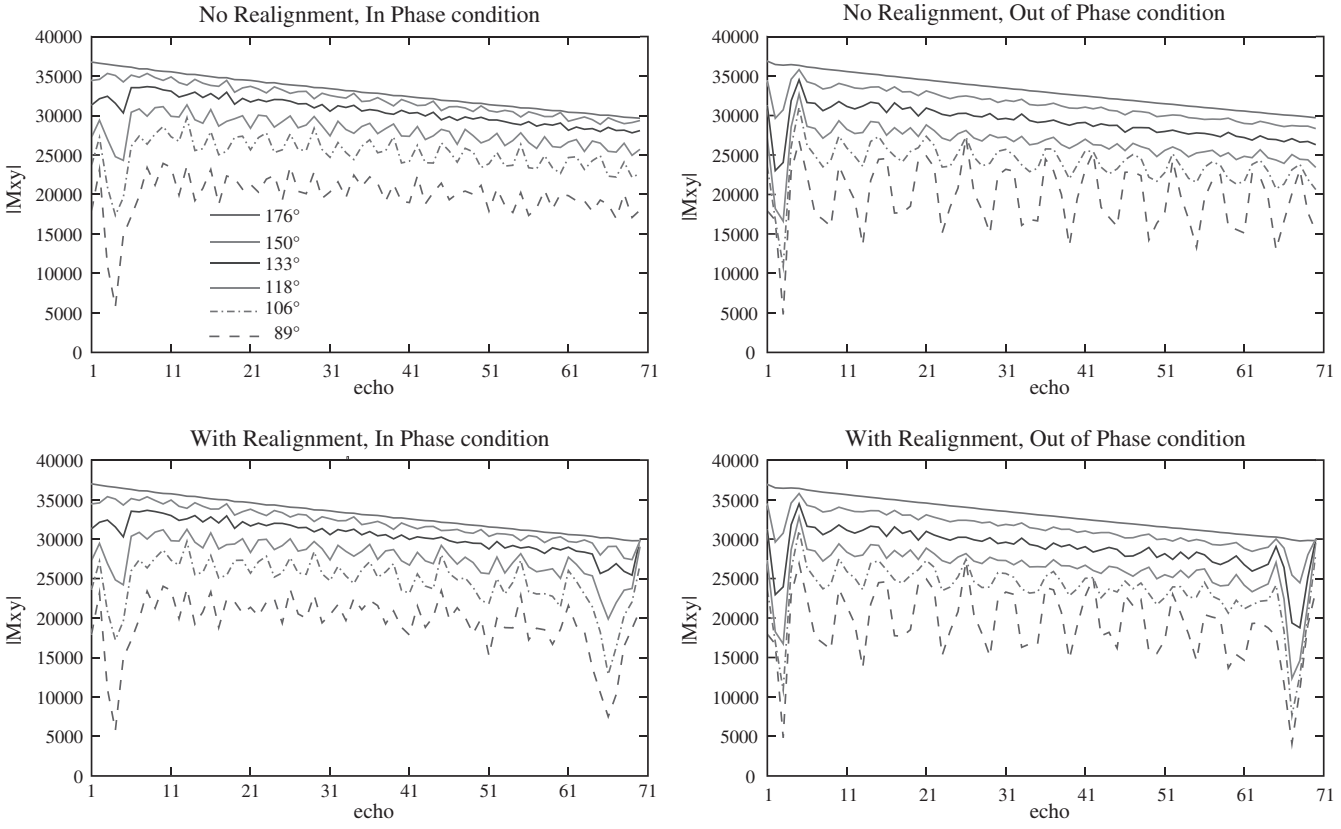

Fig. 9. The echo signal for the six nutations of Table 1, on top row with the original modulation, on bottom row with a modulation which, from echo 35 to echo 70 has been changed to permit realignment. Realignment which appears to be quite effective for nutation above 133° and still significant at 118°, and visible at 89°.

Table 4
The last echo signal magnitude, for different nutation angles, vertically, for the two initial condition 'in-phase' (In) and out-of-phase (Out), and for trains with realignment (with) or without (no). This shows that the realignment is quite effective for nutation above 133° because the magnetization obtained is close to the magnetization obtained for the 180° case (bold face values). It is still significant at 118°, within 3% of the maximum.

Last echo signal	In – with	In – no	Out – with	Out – no
176°	**29,797**	29,658	**29,801**	29,722
150°	**29,785**	29,359	**30,023**	28,348
133°	**29,935**	28,092	**29,957**	26,304
118°	29,030	25,722	29,551	23,420
106°	26,729	22,664	28,189	20,626
89°	20,985	18,015	23,434	15,332

To determine the actual nutation angles used during the experiment the signal data were fit to the simulated response, with the parameter corresponding to the master nutation angle (168°, top row, left column of Table 1) changed manually, keeping the a priori known ratio of nutations between successive experiments. It was not possible to fit perfectly the first response (highest nutation angle) nor the last (lowest nutation angle) with the given common ratio. Hence we had to increase substantially the nutation angle of the first experiment and decrease the nutation of the last experiment. But the other four data sets, and particularly the second to fourth, were fit very well (see Fig. 10, top row). The bottom row of Fig. 10 also shows that the nutation angle is a relatively sensitive parameter, so that the values of this parameter obtained by the fitting are closely determined. The uncertainty is in an interval of ±2°.

3.3. Inferring the influence of relaxation

If it is now assumed that the proposed modulation gives magnetization responses conforming to the theory, it is interesting to explore by simulation what would have been the results of some experiments more difficult to realize. Fig. 11 shows what would be the magnetization distribution along the free precession axis ωT, at the end of the train, at echo number 70, when using realignment. The left column is relative to the condition where relaxation effects are negligible, with $T_1 = \infty$, and with T_2 very long compared to the duration T_{acq} of the echo train, and for all the three possible initial magnetization states. The nutation angle of the refocusing pulses used in the simulation is 133°, a value for which, the experiments has shown, still produces a good realignment, but representing also the limit of degraded responses. One appreciates that the original magnetization is quite well restored for all conditions. The residual is probably due to imperfections in the stabilization and realignment. One notes that this residual is anti-symmetric around $\Omega = 0$ and $\Omega = \pi$. One can continue by exploring the case where the transverse relaxation time T_2 is in the order of the echo train duration T_{acq}. To simplify the analysis one can always consider that $T_1 = \infty$, knowing that one can always apply an isotropic contraction of the magnetization to take into account the influence of a finite T_1: the recovery of the longitudinal

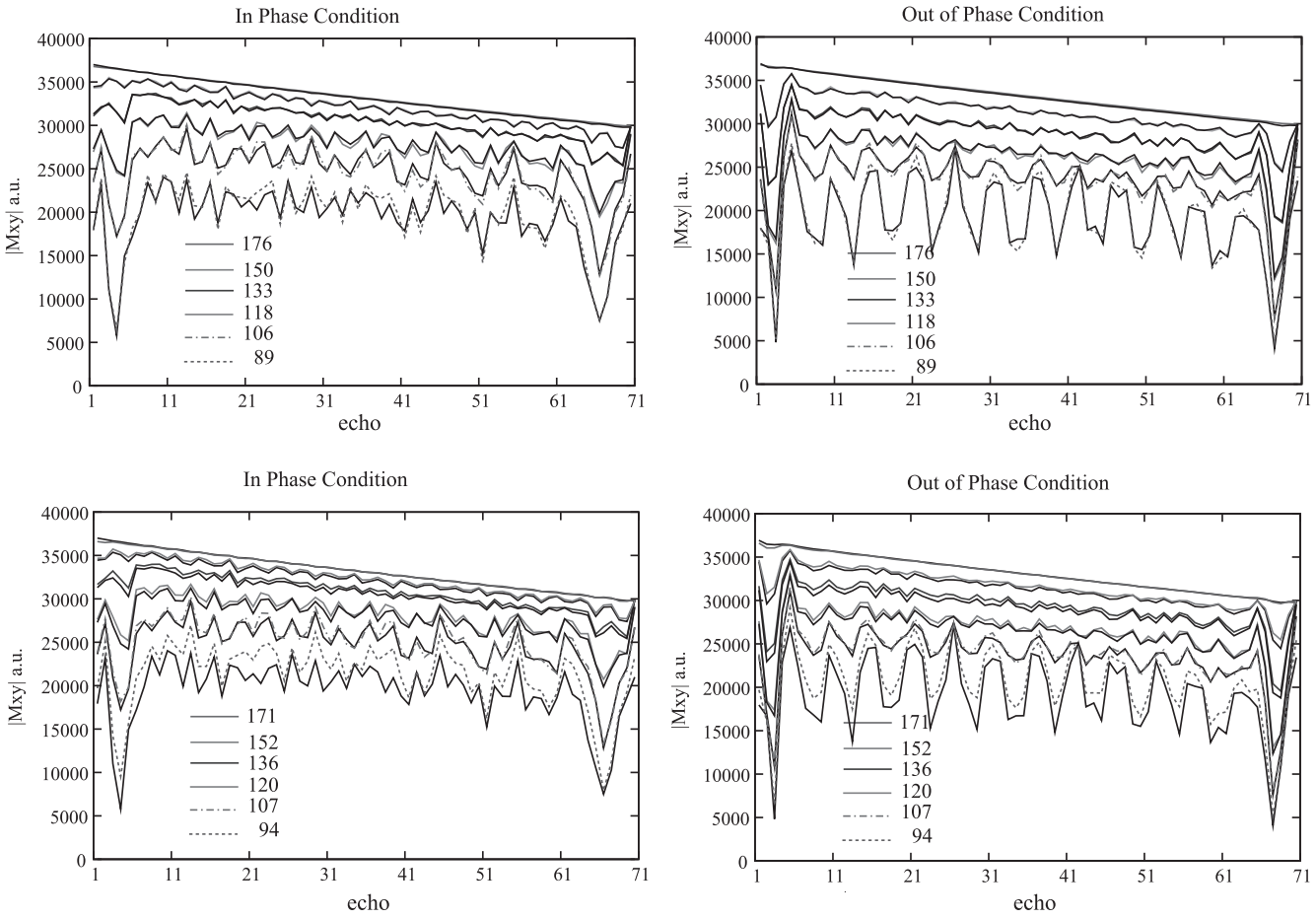

Fig. 10. The nutations of Fig. 9 where determined by fitting the responses obtained by simulation against the experimental data in case of realignment, represented here by continuous black curves (which thus reproduce the diverse curves of the bottom row of Fig. 9). The ratio between nutation angle were not changed except for the two extreme nutations as explained in Table 1. One can appreciate on the top row a very good concordance between theory and experimental results down to 118°. In the second row, the nutation angles have been voluntary changed slightly from optimum, as indicated. This shows that the sensitivity over nutation angle is rather high, and thus the values of the optimal nutation angle in the first row are well determined.

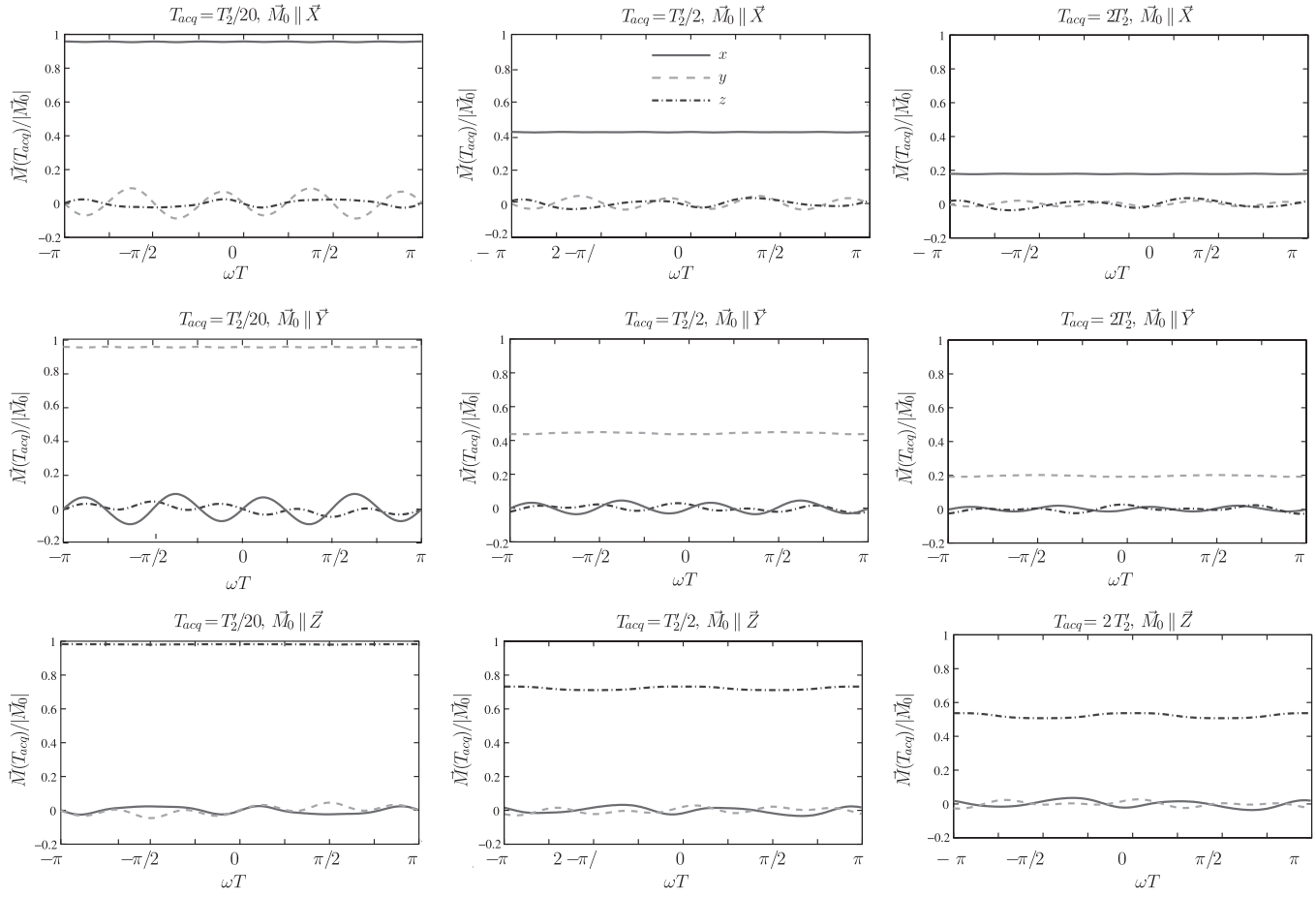

Fig. 11. Magnetization state (three components x, y, z) distribution as a function of the free precession offset ωT, at the last echo (the simulation was done with 70 echoes and T_{acq} is the echo time of the seventieth echo) for a realigned train, and for different initial magnetization, $\vec{X}$ on the first row, $\vec{Y}$ on the second, $\vec{Z}$ on the third. The nutation angle of the refocusing pulses was kept constant, 133°, but the anisotropic relaxation time T_2' given by $1/T_2' = 1/T_2 - 1/T_1$ was decreased, from $20T_{acq}$ on the left column to $2T_{acq}$ on the middle column and $T_{acq}/2$ on the right column. In all cases the longitudinal relaxation was considered nonexistent, but it can be taken into account in the form of a global scaling. Noticeably the realignment is not much perturbed, as the secondary components are reduced to the same relative level, but as expected a reduction of the three components due to relaxation is observed.

component during the train can be neglected, if T_1 is in the order of, or greater than, the duration T_{acq} of this train. One thus just applies a transverse relaxation with a rate $R_2' = R_2 - R_1,\ R_1 = 1/T_1,\ R_2 = 1/T_2$ and no longitudinal relaxation. The middle column shows the end state when the transverse relaxation rate is such that $R_2'T_{acq} = 0.5$, corresponding to an attenuation $\exp(-R_2'T_{acq}) = 0.61$. One can appreciate the good realignment stability, but of course a reduction in the principal components due to relaxation. The third column shows the same end state for $R_2'T_{acq} = 2$, (corresponding to $\exp(-R_2'T_{acq}) = 0.13$). Again the realignment is not much perturbed, only a small undulation appears on the principal components of the refocused magnetization. One notes also that the action of relaxation on the transverse original components (first and second row) is less than expected, probably due to the portion of time the magnetization, assumed to be close to $\vec{x}$ or $\vec{y}$ is tilted towards $\vec{z}$. Conversely, the effective reduction of longitudinal components, third row, is more than expected: if it stayed along the $\vec{z}$ direction no relaxation would be expected as $T_1 = \infty$. The relaxation is due to the tilting of the magnetization away from $\vec{z}$ during the train, the transverse component then being reduced with rate R_2'. Still, it is astonishing that these differential relaxations do not perturb by anisotropy the realignment process. A more careful study of the trajectories during the train will have to be conducted to better understand this result. Meanwhile one can, by simulation, determine a phenomenological value of the effective principal relaxation rates. By that it is meant relaxation rate $\widehat{R}_2$, respectively $\widehat{R}_1$, able to represent the attenuation at the last echo of the *principal* component of a magnetization originally on $\vec{x}$ or $\vec{y}$, respectively $\vec{z}$, disregarding the residual components. Hence

$$\exp(-\widehat{R}_2 \mathrm{Tacq}) = M_x(\mathrm{Tacq}), \qquad \text{when } \vec{M}(0) = \vec{x} \tag{5}$$

$$\exp(-\widehat{R}_1 \mathrm{Tacq}) = M_z(\mathrm{Tacq}), \qquad \text{when } \vec{M}(0) = \vec{z} \tag{6}$$

Fitting the preceding simulation results and some others not shown, one finds a compact mathematical expression for $\widehat{R}_1$ and $\widehat{R}_2$ which stays within 1.5% of simulated response, if $\theta > 130°$. They are

$$\widehat{R}_2 = (1 - c^2)R_2 + c^2R_1 \tag{7}$$

$$\widehat{R}_1 = (1 - 2c^2)R_1 + 2c^2R_2 \tag{8}$$

with $c = \cos\theta/2$, which for $\theta > 130°$ is approximately $c \simeq (\pi - \theta)/2$.

4. Discussion

The results concerning the relaxation influence show that under clinical conditions where transverse relaxation rate R_2 is five to ten times higher than the longitudinal relaxation rate R_1, the realignment presents an interest only if the length of the acquisition

T_{acq} is short enough compare to T_2. Typically it should be in the order of one half T_2. This is obviously true if one wants to recover the transverse magnetization remaining at the end of the train, by applying a $-(\pi/2)_y$ pulse (assuming the excitation has been $(\pi/2)_y$ pulse). Indeed, to be useful, this sort of classical driven equilibrium [19,20] must have some transverse magnetization to restore along $\vec{z}$, which will not be the case if $Tacq \gg T_2/2$. Another, more novel, application of realignment is to keep as much as possible of the longitudinal magnetization left by the flip pulse, and transferred to the distribution $\vec{W}(\omega T)$. In this setting, the flip pulse is reduced and adapted to the acquisition time *Tacq*, the inter excitation recovery time and T_1, in a manner similar to Ref. [21]. There is no useful T_1 recovery present during the train of refocusing pulses but, at least in the ideal case of 180° refocusing pulse, the longitudinal magnetization decreases with a relaxation rate R_1, and realignment of this longitudinal magnetization can substantially reduce the necessary recovery time. But in the presence of refocusing angle error which, as just shown, injects some T_2 relaxation into the magnetization $\vec{W}(\omega T)$, the acquisition window should not be extended much above $T_2/2$. Some of the co-authors have tried to apply this concept of longitudinal magnetization realignment coupled with small tip angle excitation, to hyper-polarized ^{13}C *in vitro* experiments ($T_1 = T_2$) [13] with some success. Conversely, subsequent *in vivo* experiments were not so encouraging. This is currently under investigation.

5. Conclusion

In summary the work presented here is of great interest with respect to technical applications of magnetic resonance, and may eventually be useful in some clinical settings. On the theoretical level, the present work relies on a symmetry property in the frequency domain and it may bring to mind the already known results pertaining to symmetric pulses or train of pulses [22,23]. However, a careful examination makes one realize that a symmetric pulse in the time domain presents indeed a symmetry in the frequency domain for its rotation axis but that its rotation angle is, on the contrary, anti-symmetric. In this work the symmetry of the rotation represented by the eigenfunction is complete, whether this eigenfunction is expressed by spinor components $u(\omega T)$, $v(\omega T)$ as in Ref. [8] or in the form of the transformed vector $\vec{U}(\omega T)$, $\vec{V}(\omega T)$, $\vec{W}(\omega T)$, i.e. the axis of rotation is symmetric *and* the rotation angle is symmetric. But still the two kinds of work can be related. The symmetry of the eigenfunction $\vec{U}(\omega T)$, $\vec{V}(\omega T)$, $\vec{W}(\omega T)$ comes from the fact that it represents the rotation of a full cycle of quadratic phase modulation. This cycle of quadratic phase modulation can indeed be made time symmetric with a suitable zero frequency setting, making it canonical as above. Hence from Refs. [22,23] this cycle rotation has an axis which is symmetric, but still a rotation angle which is antisymmetric. However if the cycle is long enough, we know from Ref. [8] that the rotation angle of such a train is close to either π or 2π! One has then just to remark that $-\pi = \pi(2\pi)$ or $0 = -0$, to convert a (pure) antisymmetry into an (approximate) symmetry! Careful examination of the demonstration in Ref. [8] of this cycle rotation result shows that it relies on a result from the *SLR* algorithm [24] which states that the spinor representing a finite train of pulses has a Fourier transform (virtual time domain) which is also finite (FIR filter).

Acknowledgments

The 3T MR system of CHU de Nancy Brabois where the experiments were performed, was financed in part by FEDER (Fonds Europeens de Developpement Regional). The first and last authors would like to thank the whole medical and technical staff of the Radiology Department for their kind support.

Appendix A. The spinor distribution is symmetrical around 0 for the canonical sweep

The rotation from echo i to echo $i+1$ is written in spinor form

$$\vec{x}_i(\omega T) = \begin{bmatrix} cZe^{j\delta_i} & -js \\ -js & cZ^{-1}e^{-j\delta_i} \end{bmatrix} \vec{x}_{i-1}(\omega T)\ i = 1\ldots \tag{9}$$

This is the equivalent of Eq. (7) in Ref. [8] with $Z = \exp(j\omega T)$, $c = \cos(\theta)$, $s = \sin(\theta)$.

For the particular choice of modulation (3) this becomes:

$$\vec{x}_i(\omega T) = \begin{bmatrix} jce^{j\Omega_i} & -js \\ -js & -jce^{-j\Omega_i} \end{bmatrix} \vec{x}_{i-1}(\omega T) \tag{10}$$

where we used the notation

$$\Omega_i = \omega T + i\Delta - \Delta/2 \tag{11}$$

The eigenfunction $\vec{u}$ is by definition the spinor function which is multiplied by $-j$ and translated by $-\Delta$ from one echo to the next, i.e. such that $\vec{x}(\omega T) = (-j)^i \vec{u}(\omega T + i\Delta)$ is solution of (10), or

$$-j\vec{u}(\Omega_i + \Delta/2) = \begin{bmatrix} jce^{j\Omega_i} & -js \\ -js & -jce^{-j\Omega_i} \end{bmatrix} \vec{u}(\Omega_i - \Delta/2) \tag{12}$$

This must be verified for every ωT, thus it must be verified at a given echo i for any Ω, and after simplification by $-j$

$$\vec{u}(\Omega + \Delta/2) = \begin{bmatrix} -ce^{j\Omega} & s \\ s & ce^{-j\Omega} \end{bmatrix} \vec{u}(\Omega - \Delta/2) \tag{13}$$

This is the equation of definition of the eigenfunction $-j$ (from which all other can be deduced) and is the equivalent of the definition in Ref. [8], but where the offset $\Delta/2 + \pi/2$ have been added to the linear sweep.

If one makes the supposition that, for a given value Ω_0, one has two vectors $\vec{u}(\Omega_0 - \Delta/2) = u_1$ and $\vec{u}(\Omega_0 + \Delta/2) = u_2$, solutions of the eigenfunction definition (13), centered around Ω_0, then expressing the second member of (13) in function of the first member one finds (the matrix is unitary)

$$\vec{u}(\Omega_0 - \Delta/2) = \begin{bmatrix} -ce^{-j\Omega_0} & s \\ s & ce^{j\Omega_0} \end{bmatrix} \vec{u}(\Omega_0 + \Delta/2) \tag{14}$$

showing that $\vec{u}_1$ and $\vec{u}_2$, in reverse order, are also the solutions of (13) centered around $-\Omega_0$. This shows (for instance by changing Ω_0 into $-\Omega_0$ in (14)) that if $\vec{u}(\Omega)$ is solution, then $\vec{u}(-\Omega)$ is also solution, so $\vec{u}(\Omega)$ may be made symmetric. There may be solutions which are non symmetric, but the smoothest one that is retained by the algorithm presented in Ref. [8] is this symmetric solution. Because the distributions $\vec{U}(\omega T)$, $\vec{V}(\omega T)$, $\vec{W}(\omega T)$ are deduced locally from $\vec{u}(\omega T)$ by the density matrix equation, they are also symmetrical.

References

[1] H.Y. Carr, E.M. Purcell, Effects of diffusion on free precession in nuclear magnetic resonance experiments, Phys. Rev. 94 (1954) 630–638.
[2] T. Gullion, D.B. Baker, M.S. Conradi, New, compensated Carr–Purcell sequences, J. Magn. Reson. 89 (1990) 479–484.
[3] A.A. Maudsley, Modified Carr–Purcell–Meiboom–Gill sequence for NMR Fourier imaging applications, J. Magn. Reson. 69 (1986) 488–491.
[4] P. Le Roux, G. McKinnon, Non CPMG fast spin echo with full signal, in: Proceedings of the Sixth Annual Meeting of ISMRM, Sydney Australia, 1998, p. 574.
[5] J.B. Murdoch, An "effective" method for generating spin-echo intensity expression, in: Proceedings of the Second SMR Scientific Meeting, San Francisco CA, 1994, p. 1145.

[6] Y. Zur, M.L. Wood, L.J. Neuringer, Spoiling of transverse magnetization in steady-state sequences, Magn. Reson. Med. 21 (1991) 251–263.
[7] P. Le Roux, Progress in non-CPMG fast spin echo, in: Proceedings of the Seventh Annual Meeting of ISMRM, Philadelphia PA, 1999, p. 7.
[8] P. Le Roux, Non-CPMG fast spin echo with full signal, J. Magn. Reson. 155 (2002) 278–292.
[9] M.E. Bastin, P. Le Roux, On the application of Non-CPMG SSFSE sequence to diffusion tensor MRI of the human brain, Magn. Reson. Med. 48 (2002) 6–14.
[10] S. Chabert, N. Molko, Y. Cointepas, P. Le Roux, D. Le Bihan, Diffusion tensor imaging of the human optic nerve using a non-CPMG fast spin echo sequence, J. Magn. Reson. Imag. 22 (2006) 307–310.
[11] A. Oner, T. Tali, F. Celikyay, A. Celik, P. Le Roux, Diffusion weighted imaging of the spine with a non-Carr–Purcell–Meiboom–Gill single-shot fast spin-echo sequence:initial experience, Am. J. Neuroradiol. 28 (2007) 575–580.
[12] P.H. Le Roux, Y.-F. Yen, Return to equilibrium after a non-CPMG spin echoes train, Magn. Reson. Mater. Phys. Biol. Med. 22 (Suppl. 1) (2009) 83–84 (Abstract No. 114).
[13] Y.-F. Yen, P.H. Le Roux, D. Mayer, A. Takahashi, J. Tropp, D. Spielmnan, A. Pfeffebaum, R. Hurd, Exploring multi-shot non-CPMG for hyperpolarized 13C metabolic MR spectroscopic imaging, in: Proceedings of the Joint Annual Meeting ISMRM-ESMRMB 2010, Stockholm, Sweden, 2010, file 1015-4209.pdf.
[14] P.H. Le Roux, First order catalyzing of the non-CPMG sequence, in: Proceedings of the 17th Annual Meeting of ISMRM, Honolulu, HI, USA, 2009, p. 2657.
[15] P.H. Le Roux, Inversion of a non-CPMG fast spin echo train, in: Proceedings of the Joint Annual Meeting ISMRM-ESMRMB 2010, Stockholm, Sweden, 2010 (file 3035-3072.pdf).
[16] D.G. Norris, P. Bornert, T. Reese, D. Leibfritz, On the application of ultra-fast RARE experiments, Magn. Reson. Med. 27 (1992) 142–164.
[17] D.C. Alsop, Phase insensitive preparation of single-shot RARE: application to diffusion imaging in humans, Magn. Reson. Med. 38 (1997) 527–533.
[18] P. Le Roux, Non-CPMG phase modulation, the easy way, in: Proceedings of the 14th Annual Meeting of ISMRM, Seattle, 2006, p. 3368.
[19] E. Becker, J. Feretti, T. Farrar, Driven equilibrium Fourier transform spectroscopy. a new method for nuclear magnetic resonance signal enhancement, J. Amer. Chem. Soc. 91 (1990) 7784.
[20] R.R. Ernst, G. Bodenhausen, A. Wokaun, Principle of Nuclear Magnetic Resonance in One and Two Dimensions, Oxford University Press, Oxford, 1988.
[21] R.R. Ernst, W.A. Anderson, Application of Fourier transform spectroscopy to magnetic resonance, Rev. Sci. Instrum. 37 (1966) 93–102.
[22] J.T. Ngo, P.G. Morris, NMR pulse symmetry, J. Magn. Reson. 74 (1987) 122–133.
[23] A. Shaka, A. Pines, Symmetric phase-alternating composite pulses, J. Magn. Reson. 71 (1987) 495–503.
[24] J. Pauly, P. Le Roux, D. Nishimura, A. Macovski, Parameter relations for the Shinnar–Le Roux selective excitation pulse design algorithm, IEEE Trans. Med. Imaging 10 (1991) 53–65.